PRELIMINARY AERODYNAMIC INVESTIGATION OF AN UNMANED BOX-WING AIRCRAFT

M. Martínez*, C. Cuerno*
***Universidad Politécnica de Madrid**
mmartinezrodriguez0@alumnos.upm.es; cristina.cuerno@upm.es

Keywords: *box-wing, aerodynamics, vortex-lattice*

Abstract

The box-wing aircraft concept is that built from two wings, usually of the same span, connected by their tips with vertical surfaces.

Induced drag reduction theory is highlighted and the concept is aerodynamically investigated through several geometric parameters. Vortex-Lattice method is employed for such purpose.

Analysis of the main aerodynamic magnitudes with the angle of attack variation under the parameters' evolution is done. Moreover, attention has been paid on the comparison between box-wing and its equivalent monoplane.

1 Introduction

In order to reduce the over-increasing fuel costs and CO_2 emissions of transport airplanes, the designers are reconsidering different unconventional configurations that were proposed and discarded many years ago [1]. This effort is also being developed due to the fact that the conventional configuration is approaching its limit in productivity and capacity at a size around that of the Airbus A380 [2].

A number of configurations have been proposed in the past [3], which can be indentified in terms of two variables: the number and position of lifting-surfaces (canard, tandem, classical, three-surface, joined-tips and tailess) and the solution selected for allocating the payload (one/two fuselages, partially inside the fuselage and the wing, and completely in the wing). By the combination of one of each variable, there is a different aircraft configuration, maybe being the biplane the first of all them. Several studies were done and some progress was achieved, pointing out that aerodynamic performance could improve, overcoming that of the monoplane if the wings were placed properly. However, research efforts were mainly devoted to the monoplane because of the steps forward made in the materials and engine areas.

Among those possible configurations obtained in the previously described procedure, a special interest is paid nowadays to the lay-outs in which the lifting surfaces (typically wing and horizontal tailplane) are connected. The most general configuration in this category is the so-called "box-wing". It is the purpose of this study to deep in the aerodynamic knowledge of that configuration.

2 Literature review

Nowadays, for civil transport airplanes, when performing cruise conditions, induced drag contributes around 43% of the total drag during cruise flight [4].

Aerodynamic drag can be defined as the sum of its parasitic, induced and compressibility components. Induced drag can be formulated as:

$$C_{Di} = \frac{{C_L}^2}{\pi e AR} \qquad (1)$$

Examining this formula, two ways of reducing the induced drag arise; on the one hand, an option is to increase the aspect ratio of the wing. This could provoke structural issues due to the loads increasing in a beam-like structure highly loaded already. On the other hand, is to look for higher values of the Oswald efficiency factor. For monoplanes, however, the

maximum value is the unity, reached with an elliptic lifting distribution and without lift-dependent skin friction drag.

Non-planar configurations, such as the box-wing, take advantage of those two approaches. They can afford the higher structural exigency derived from the aspect ratio increase by distributing this increment in more than one lifting surface. In addition to that, higher Oswald efficiencies than one can be reached by them. Next figure shows the span efficiency, that is, the ratio between the induced drag of the monoplane and the induced drag of a nonplanar system of the same span and lift, for several systems with the same height to span value. Thus, box-wing shape reaches the maximum possible reduction in induced drag by means of connecting the wing tips to the stabilizer tips through some vertical elements [5].

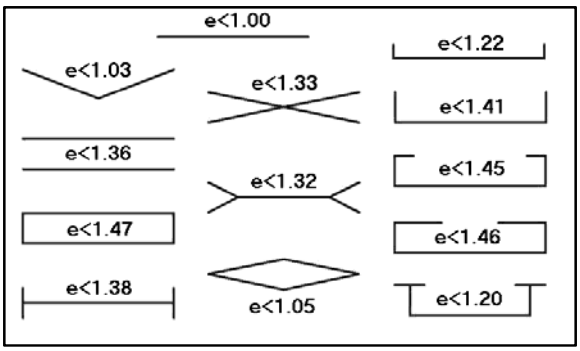

Fig. 1. Span efficiency for various optimally loaded nonplanar systems. 20% height to span ratio. [5]

The original idea was proposed by Prandtl in 1920 [6] and it is being reconsidered nowadays also under the name of Prandtlplane [4]. Prandtl found that the biplane has a lower drag than an equivalent monoplane and its minimum drag is obtained when the two wings of the biplane have the same span. Further on, more induced drag reduction can be achieved if wing end-plates are attached to the wingtips, thus making a closed system (box). In a very simplified way, this effect is due to the fact that the presence of the wingtips causes a reduction in the net induced velocity in the downwash of each wing. Hence, the induced angle of attack is decreased for the same total lift, reducing the induced drag which is proportional to the magnitude of the induced velocities in the downwash [7].

Previous research was conducted mainly in the field of the biplanes. Two-dimensional [8] and three-dimensional [9-12] tests were performed in the past, showing that locating the upper wing ahead of the lower one increases the lift to drag ratio and reduces the pressure centre travel thus softening the stability problem. Important reduction in drag was observed too in these experiments.

Winglets were added to the biplane system [7], investigating the configuration both theoretically and experimentally but focusing in a few configurations only. In the present work, the box-wing configuration is being analyzed for an unmanned air vehicle in the mini-category from a numerical point of view after some experimental research done before, which was published elsewhere [13].

Considering the fact that the flight of most UAS takes place at low Reynolds numbers, it was considered necessary to study the aerodynamics of the box wing configuration by testing different models in a wind tunnel to be able to obtain reasonable results, and the results were presented in [13]. That study was enhanced by varying not only the sweepback angles of the two wings, but also their position along the models' fuselage. Certain models showed a more efficient behaviour than others, pointing out that certain relative positions of the wing exist that can improve the aerodynamics efficiency of the box wing configuration. Nevertheless the conclusions of the study were not as conclusive as it was originally expected and this fact has motivated this new approach, together with the lack of theoretical/numerical results in open literature for box-wing aircraft configurations flying in the low Reynolds number regime.

A numerical analysis has been performed in order to understand the behaviour of the box-wing configuration, varying the main parameters that define a box-wing layout through the utilization of aerodynamic codes.

Vortex-Lattice codes have been applied at a first stage, obtaining lift-to-induced drag versus lift curves where the effect of the parameters variation is observed.

3 Problem stating

Current research aims to understand the effect of varying the main geometric parameters which define the non-conventional aircraft concept called box-wing, focusing mainly in core aerodynamics magnitudes like lift and drag coefficients and its related lift to drag efficiency ratio.

The parameters selected are the following:

- Gap (*Ga*). It is the vertical separation distance between the leading edges of both the upper and lower wings perpendicular to the free stream, divided by the chord length.
- Stagger (*St*). It is the longitudinal separation distance between the wings' leading edges, parallel to the free stream. It is positive when the upper wing is ahead of the lower wing.

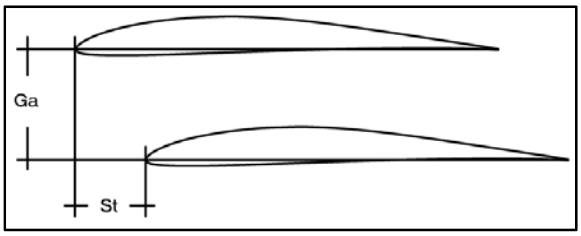

Fig. 2. Gap and stagger definition.

- Decalage (*De*). The relative angle between the mean wings' chords. It is positive when the upper wing is at higher angle of incidence than the lower one.

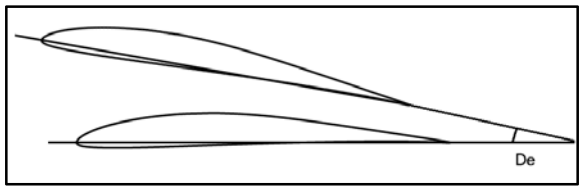

Fig. 3. Definition of Decalage.

- Aspect ratio (*AR*). Defined as the ratio between wingspan and the average wing chord.
- Sweep (Λ). It is the angle between the imaginary quarter-chord line with another one normal to the plane of symmetry.
- Areas' relationship (ξ). It is the ratio between the upper wing's surface and the lower one. In particular:
  - $S_{UW} = \xi \cdot C \cdot b$
  - $S_{LW} = (2 - \xi) \cdot C \cdot b$

4 Problem approach

The Vortex-Lattice method (VLM) has been employed as the tool to obtain the aerodynamics characteristics. VLM are a subset of computational fluid dynamics tools. The flow is considered potential, being applicable the Laplace equation. One of its solutions is the vortex line. From this, it is possible to build a horse-shoe vortices grid over the lifting surfaces.

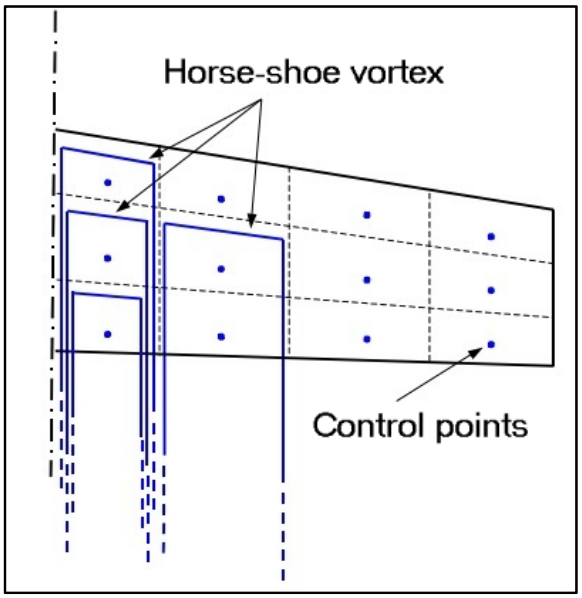

Fig. 4. Lifting surface modelling with horse-shoe vortices.

Lift and induced drag are calculated integrating the forces of each vortex. This calculation, including induced angles, is inviscid and linear thus independent from wing's speed and air's viscous characteristics. Geometry and boundary conditions (i.e. flow must be tangent to the surface panels) have a huge influence in the calculation's validity.

For the current work, Athena Vortex Lattice (AVL) [14] code has been selected. It is a VLM widely used through the aerodynamic design initial steps. It works reading a configuration

geometry from an input file, gathering also air density and speed; centre of gravity if inertial properties are considered; reference chord, wingspan and wing area. Parasitic drag cannot be calculated by AVL. If desired, it must be defined as an input parameter of the code. Compressibility drag is accounted following the Prandtl-Glauert correction.

AVL, as other VLM, should be only used for low angles of attack where stall is not suspected. This is due to the dependence of the boundary layer development not only in the streamwise pressure gradients thus making C_L a not very good parameter to account for local stall.

In addition to lift, the total drag coefficient is found by cumulative surface force integration over each lifting surface, and induced drag is calculated from the wake trace in the Trefftz plane far downstream.

The mesh covering the lifting surfaces follows a Cartesian style. It can be set both in chordwise and spanwise directions. The parameter aimed to describe the grid ranges from 3 to –3 regarding the following figure:

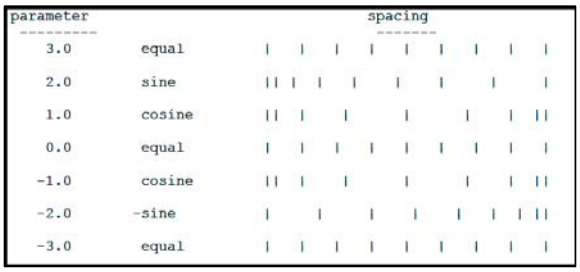

Fig. 5. Spacing relationship definitions.

Through AVL the section profile is set. It offers the possibility of introducing the coordinates of the desired airfoil and also to choose a four digit series NACA profile. It has been the case of the current research. Specifically, the NACA 0012 symmetric profile is chosen for the wings in order to limit the airfoil influence in the results constraining the analysis to the parameters' variation and leaving a proper airfoil selection and design for fore-coming investigations. In addition to that, thin symmetric airfoil NACA 0006 has been chosen for the vertical interconnecting surfaces with the same scope. It is selected a reference chord value of 30 cm, a typical value for small UAS. The same criterion is applied to the airspeed, setting it to 25 m/s.

Advantage is taken of the lift coefficient derivative with the angle of attack ($C_{L\alpha}$) correction included in AVL code which comes from potential theory. It essentially dictates the $C_{L\alpha}$ to be used by the method:

$$C_{L\alpha} = 1 + 0.77\,\frac{t}{c} \qquad (2)$$

Hereafter is depicted an example of the regular grid distributed over the lifting surfaces established by AVL editor:

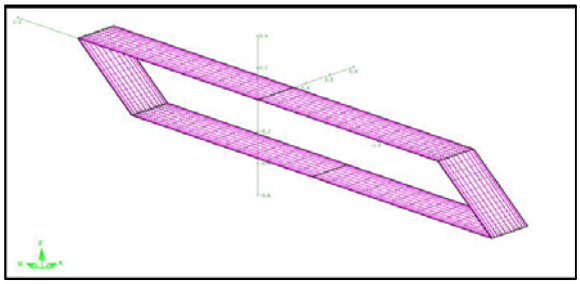

Fig. 6. Box-wing configuration built by means of AVL.

5 Analysis and results

Several box-wing configurations have been built by means of the AVL geometry input file, where also reference magnitudes, as profile chord or airspeed have been defined. In a first shot, four of the parameters described in section 3 of the present work have been considered, taking into account the following values:

Parameter	Values
Ga	{ 0.25 *C* ; 0.5 *C* ; 0.75 *C* ; 1.0 *C* ; 1.25 *C* ; 1.5 *C* ; 1.75 *C* ; 2.0 *C* }
St	{ 2.0 *C* ; 1.5 *C* ; 1.0 *C* ; 0.5 *C* ; 0.0 *C*; –0.5 *C* ; –1.0 *C* ; –1.5 *C* ; –2.0 *C* }
De	{ 0° ; –4° ; –6° ; –8° }
AR	{ 3 ; 5 ; 7 ; 10 }

Fig. 7. Main parameters variation

Combining the parameters of the table, 1152 configurations are created. They have been tested by varying both α and C_L. Angle of attack

is varied from 1° to 9° in steps of 1° while the variation with the lift coefficient is made from 0.1 to 0.9 with a 0.1 step.

The other two parameters, Λ and ξ have been added separately to these baseline configurations in order to isolate the effect of their variations with the scope of analyzing their complexity in a proper way.

5.1 Gap and stagger effects.

An overview effect of the gap variation with the angle of attack is shown below (Fig.8) for a configuration with St = 0.0 C, De = –6°and AR = 10.

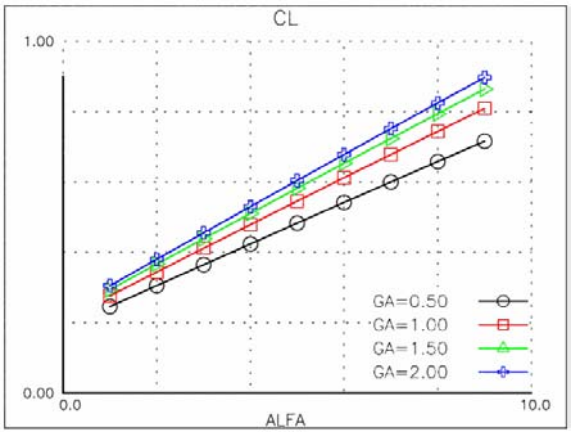

Fig. 8. C_L vs α variation with Ga

It is observed, from Figure 8, that the greater the gap is, the greater the lift coefficient becomes. That is due to the progressive loss of interaction between the wings as the gap parameter grows.

At an angle of attack of 5°, C_L = 0.48 for the Ga = 0.5 C configuration. Doubling the gap up to 1.0 C, the lift coefficient reaches the value of 0.55, that is, a 14.6 % of increment. This percentage is reduced for higher values of gap. For Ga = 1.5 C a 21.2 % increment is reached from the lower gap configuration and a 25.8 % for the case when wings are separated by a distance of two times the chord.

Keeping constant the value of the angle of attack, that is, 5°, a comparison is made cross plotting Ga and St values in Fig.9.

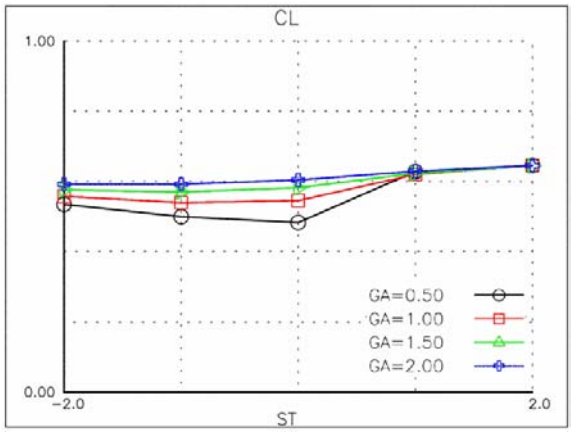

Fig. 9. C_L variation with St and Ga. (α = 5°).

C_L does not vary with any gap choice for St positive values. It suggests that a proper box-wing configuration will have a positive stagger value, at least in lift terms. In addition to the previous statement, no substantial lift coefficient gain is achieved by means of incrementing positive stagger from 1.0 C to 2.0 C.

Induced drag coefficient variations with the angle of attack are observed hereafter (Fig.10), in order to have a more complete image of the concept behaviour.

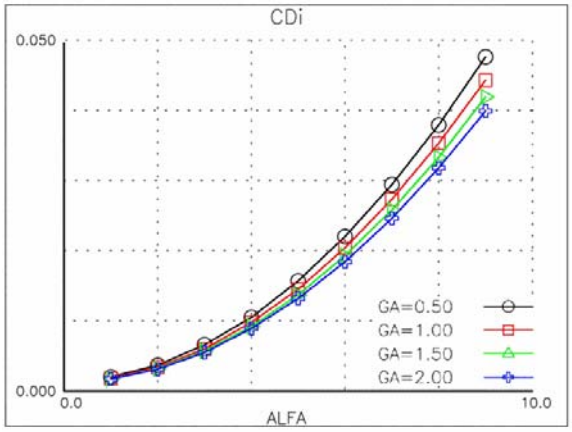

Fig. 10. C_{Di} vs α variation with Ga

It is clear that as Ga increases, C_{Di} is reduced. At of 5°, for α = 5°, Ga = 0.5C, C_{Di} = 0.016. Taking this value as reference, decrements are obtained by making Ga greater. For Ga=1.0C, induced drag coefficient is reduced in a 7.6 %. When gap reaches the higher value studied, that is, 2.0C, C_{Di} = 0.013

with a reduction in percentage from the reference value of a 15.9 %.

Repeating the process made previously for C_L, variations of C_{Di} with *Ga* and *St*, are depicted for a fixed $\alpha = 5°$ in Fig.11.

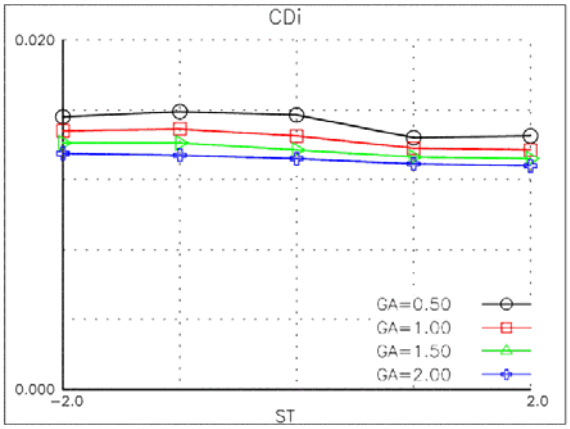

Fig. 11. C_{Di} variation with *St* and *Ga*. ($\alpha = 5°$).

A third aerodynamic magnitude, the longitudinal moment coefficient, is also analysed. Previous approaches are followed in order to carry out the study.

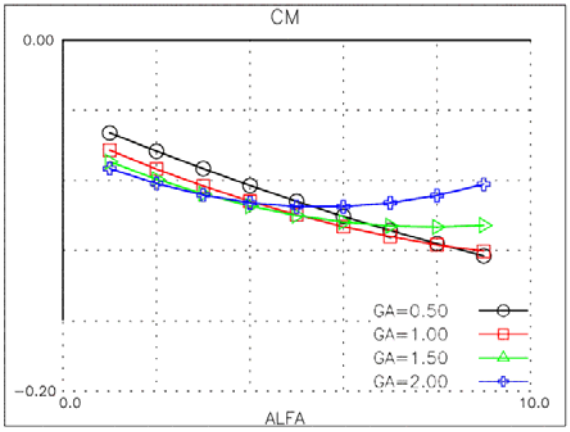

Fig. 12. C_m vs α variation with *Ga*

Behaviour of C_m has a common trend for small angle of attack values. Its slope is negative for small α values, and it is maintained negative, for $Ga = 0.5C$ and $1.0C$ up to $\alpha = 9°$, that is, the maximum angle of attack considered in order to preserve the validity of VLM results.

The benefits observed in C_L and C_{Di} in previous paragraphs must be quarantined in the light of Fig.11 outputs. However, the negative slope, that is, the longitudinal stability is guaranteed at somewhere between $Ga = 1.0C$ and $Ga = 1.5C$.

Regarding the aforementioned conclusions, C_m variations for lower gap values, between $0.25C$ and $1.25C$ and several stagger values (both positive and negative) are depicted below instead of the former approach.

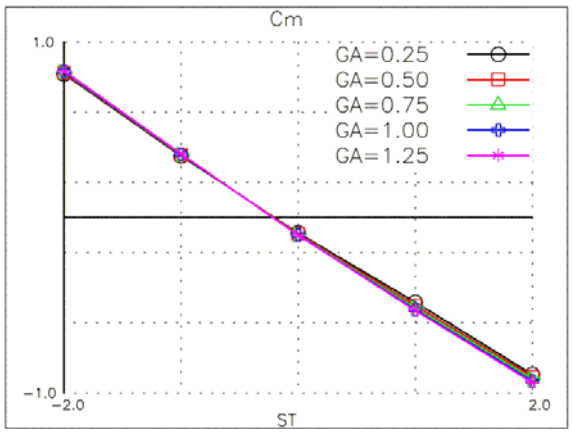

Fig. 13. C_m variation with *St* and *Ga*. ($\alpha = 5°$).

A lack of C_m variation is observed in Fig.13. In fact, fixing α to 5° and depicting C_m values for the *Ga* and *St* combinations do not give appreciable C_m change. The scale factor used in Fig.12 is erased with the *St* variation in Fig.13.

Anyway, it can be extracted from Fig.13 than negative *St* values leave a C_m higher than zero, thus making the configuration longitudinally instable and giving another argument in favour of the positive staggered configurations.

5.2 Decalage effect.

The effect of the decalage angle variations is observed in this section. It is made an approach by evaluating the aerodynamic magnitudes change with *De* for selected combinations of *Ga* and *St*. Specifically, gap values up to $1.00C$ and stagger values, both positive and negative, are regarded Figs.14 depicts C_L evolution while Fig.15 does the same for C_{Di}. Results are chosen again for $\alpha = 5°$.

Results of Fig.14 point out that a high decalage angle provides a high lift coefficient. Indeed, C_L gets greater as *De* gets more

negative. In addition to that it can be seen what was observed in previous evaluations about stagger and gap. *Ga* = 1.0*C* configurations provide greater C_L as the positive staggered configurations do.

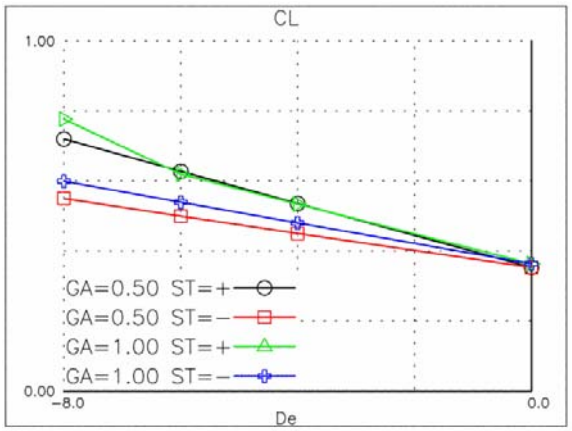

Fig. 14. C_L variation with *De, St* and *Ga.* (α = 5°).

In order to learn how *De* influences the induced drag coefficient, its evolution is regarded for several *De* angles with a configuration of *Ga* = 1.0*C* and *St* = 1.0*C*, keeping *AR* = 10.

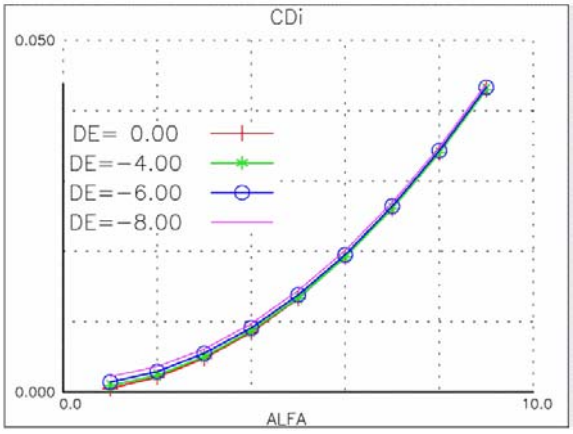

Fig. 15. C_{Di} vs α variation with *De.*

Little information can be extracted of Fig.15 except for setting that variations of *De* do not alter C_{Di} behaviour. Deeper insight should be made taking into account viscous effects because although the induced drag remains equal for *De* variations, skin friction drag is expected to change due to this effect, that is, as *De* becomes more negative, more front surface is offered to the airstream thus increasing the drag. A compromise between lift gains and viscous drag losses should be regarded in next studies.

5.3 Aspect ratio effect.

The aspect ratio, as seen section 2, has a positive effect in the induced drag reduction because of the fact that the longer a wing is, the weaker are its wingtip vortices, thus reducing the induced speed, the induced angle of attack and the induced drag.

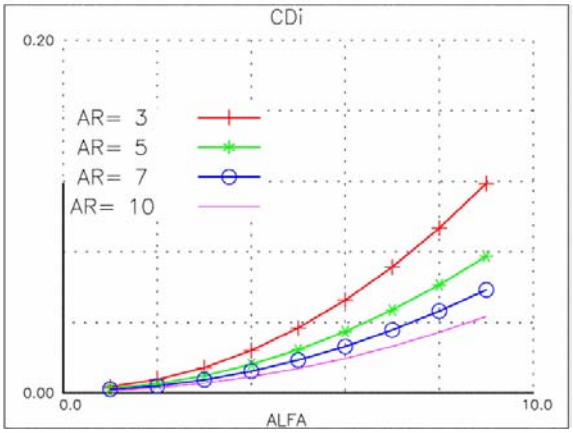

Fig. 16. C_{Di} vs α variation with *AR.*

Fig.16 shows variations of C_{Di} with α as they were expected. The greater the *AR* is, the lower the C_{Di} becomes. Benefits are not harvested by enlarging the wing to get a high *AR* because that can be done for the monoplane too. The key point will be explained in section 6 regarding the concept of the *AR* of an equivalent monoplane.

5.4 Sweep effect.

Both the upper and lower wings' sweep have been varied from 30° to −30° by steps of 10°, resulting in a humongous amount of configurations to be analysed. Several comparisons have been observed, taking into account aerodynamic coefficients variations with α as it has been done in previous sections, that is, C_L, C_{Di} and C_m.

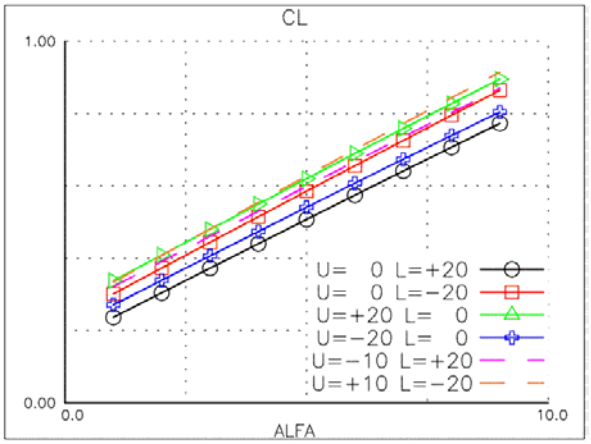

Fig. 17. C_L vs α variation with Λ.

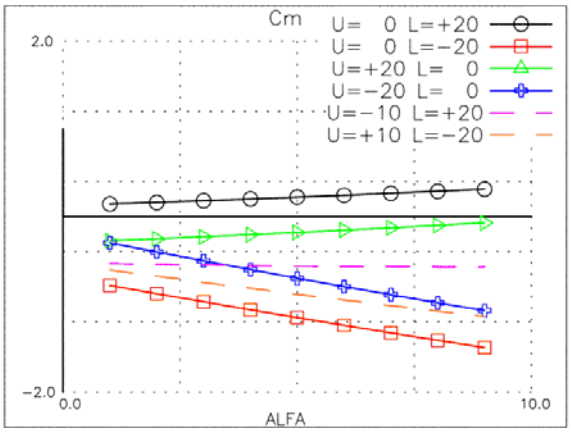

Fig. 18. Cm vs α variation with Λ.

Figs.17 and 18 represent lift and longitudinal moment variations with angle of attack for several wing sweep combinations. Aiming to provide clear pictures, not all the combinations have been depicted but considerations from them can be extracted however:

- $\Lambda_U = 0°$; C_L is lower for $\Lambda_L > 0°$ configurations. Besides that, $C_{m\alpha}>0$ thus unstable.
- $\Lambda_L = 0°$; C_L decreases for $\Lambda_U < 0°$ combinations, existing a significant break between Λ_U positive and negative values.

Regarding the previous paragraphs, $\Lambda_L < 0°$ and $\Lambda_U > 0°$ cases are evaluated altogether, observing through the C_m behaviour that for swept configurations, longitudinal stability is reached only when the difference $\Lambda_U - \Lambda_L \cong 30°$, being these configurations the best suited within a compromise between lift capability and stability.

C_{Di} evolution with the angle of attack is shown in Fig.19, for a fixed configuration of $Ga = 1.0C$, $St = 1.0C$, $De = -6°$ and $AR = 10$. Little differences are spotted with high α values but in general, no significative difference exists.

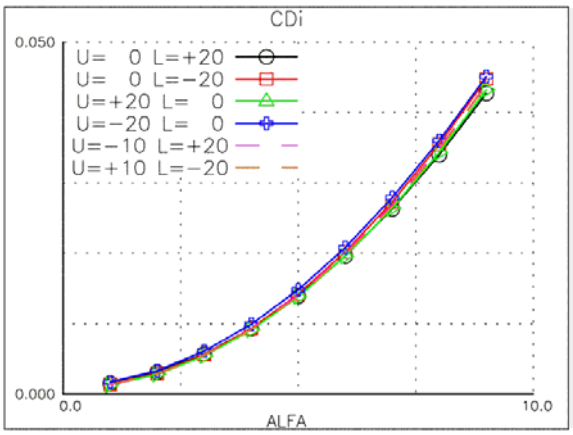

Fig.19. C_{Di} vs α variation with Λ.

5.5 Areas relationship effect.

Starting from the baseline configurations, the effect of the areas relationship has been studied.

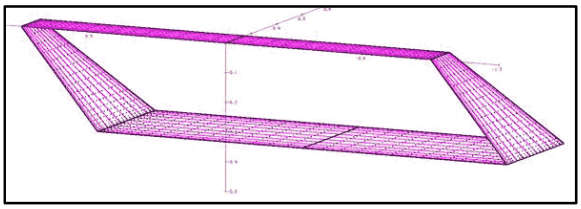

Fig. 20. Box-wing configuration with $\xi = 0.5$

New layouts (Fig.20) have been built by adding the ξ parameter in the following way (Fig.21):

Parameter	Values
ξ	{ 0.5 ; 0.75 ; 1.0 ; 1.25 ; 1.5 }

Fig. 21. ξ parameter variation

In Figs.22 and 23, the aforementioned variations are added to the configuration defined by $Ga = 1.0C$, $St = 0.0C$, $De = -6°$ and $AR = 10$. Higher C_L values are reached with lower values of ξ, that is, when the upper surface is smaller than the lower one.

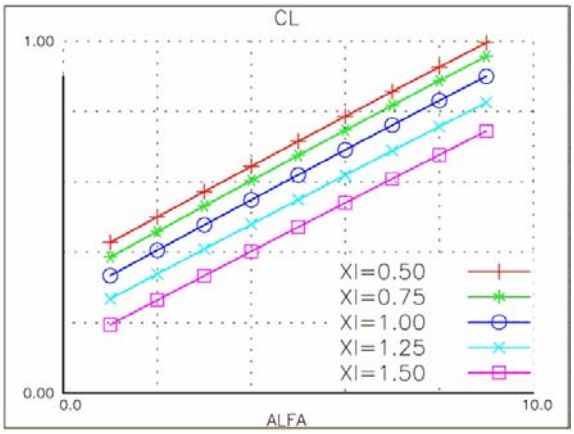

Fig. 22. C_L vs α variation with ξ.

Although no great variations are seen in the evolution of C_{Di} with α, it is weakly lower for $\xi = 1.5$ (Fig.23)

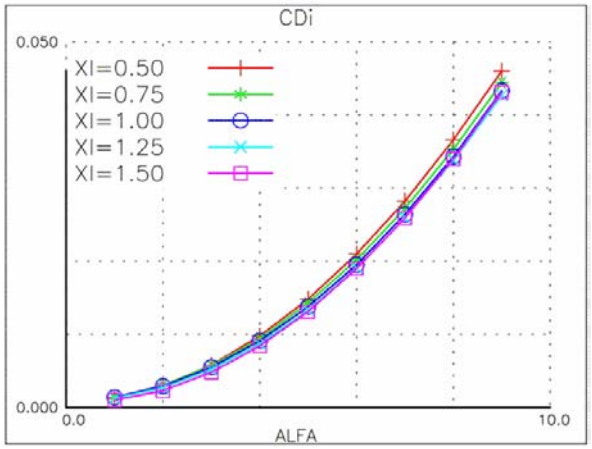

Fig. 23. C_{Di} vs α variation with ξ.

6 Equivalent monoplane comparison

In addition to the overall analysis presented in the previous section, a comparison between several baseline box-wing configurations and their related equivalent monoplanes is approached.

The induced drag of a biplane can be modelled as the induced drag of each wing plus an interference coefficient [6]:

$$D_i = \frac{{L_1}^2}{\pi q {b_1}^2} + 2\frac{\sigma L_1 L_2}{\pi q b_1 b_2} + \frac{{L_2}^2}{\pi q {b_2}^2} \qquad (3)$$

Assuming the absence of *De* and *St,* substituting lift as the product of C_L, dynamic pressure and surface and introducing some parameters ratios, previous equation turns to:

$$D_i = \frac{q {C_L}^2 S^2}{\pi {b_1}^2}\frac{(\mu^2 + 2\sigma\mu r + r^2)}{\mu^2(1+r)^2} \qquad (4)$$

Making an analogy between both the monoplane (with Oswald efficiency equal to 1) and biplane induced drag, it can be find the equivalent monoplane aspect ratio [15]:

$$EMAR = \frac{{b_1}^2}{S}\frac{\mu^2(1+r^2)}{\mu^2 + 2\mu\sigma r + r^2} \qquad (5)$$

As μ = 1 (upper and lower wing spans are equal), Prandtl's interference factor can be modelled as follows, only depending on *Ga* and *b*:

$$\sigma = \frac{1 - 0.66\frac{Ga}{b}}{1.05 + 3.7\frac{Ga}{b}} \qquad (6)$$

Taking into account that *Ga* and *AR* are defined as a factor multiplied by the reference chord, say:

$$Ga = k_g c_{ref} \quad g = 1, \dots, 8 \qquad (7)$$
$$b = k_b c_{ref} \quad b = 1, \dots, 4 \qquad (8)$$

Hence,

$$EMAR = \frac{\left(1.05 + 3.7\frac{k_G}{k_b}\right)k_b}{2.05 + 3.04\frac{k_G}{k_b}} \qquad (9)$$

Then, keeping the box-wing area constant for the equivalent monoplane, it is possible to obtain its chord and span in order to built these monoplanes:

$$c_M = \sqrt{\frac{2k_b}{EMAR}}\,c_{ref} \qquad (10)$$

$$b_M = EMAR \cdot c_M \qquad (11)$$

It has been chosen a typical C_L value of 0.3 accordingly to those of an UAV in the small category. Then, the 8x4=32 different

monoplanes are tested, in terms of C_{Di}, against their box-wing counterparts.

Best reduction percentage is hold by the following configuration:

- $Ga = 0.25C$
- $St = 0.5C$
- $De = -6°$
- $AR = 10$
- $\xi = 1.5$

This configuration reduces its C_{Di} with respect to its equivalent monoplane by a 24.8 %.

The general trend of the parameters points out that the best suited configurations for the reduction of the induced drag are those whose parameters are among:

- $Ga = 0.25C$; $0.5C$
- $St = 0.5C$; $1.0C$
- $De = -4°$; $-6°$
- $AR = 7.5$; 10
- $\xi = 1.0$; 1.5

7 Conclusions

A deep study of the box-wing concept has been preformed, evaluating its aerodynamic characteristics, by means of VLM, trough the variation of the geometric parameters of the configuration.

Positive St configurations behave better in terms of C_L and C_{Di}. The same occurs for high values of Ga, although longitudinal stability is not achieved for $Ga > 1.25\ C$.

C_L becomes high as De gets more negative and ξ smaller. Both parameters have negligible influence on $C_{Di.}$

A good compromise between lift capability and longitudinal stability is reached when the difference $\Lambda_U - \Lambda_L \cong 30°$.

Future work is expected in the line of an experimental approach, taking advantage of UPM wind tunnel test facilities of "Tecno-Getafe".

References

[1] Cuerno-Rejado C, Alonso-Albir L, Gehse P. Conceptual design of a medium-sized joined-wing aircraft. *Proc. IMechE, Part G Journal of Aerospace Engineering*, Vol. 224, pp. 681-696, 2010.

[2] Vigneron Y. Commercial aircraft for the 21st century – A380 and beyond. *Proceedings of the AIAA/ICAS International Air Symposium and Exposition,* Dayton, Ohio, USA, AIAA Paper 2003-2886, 2003.

[3] Torenbeek E. Introductory overview of innovative civil transport aircraft configurations. *Innovative configurations and advanced concepts for future civil aircraft. Lecture Series 2005-2006,* (Eds. E. Torenbeek and H. Deconinck), 2005, von Karman Institute, Brussels, Belgium.

[4] Frediani A, Rizzo E, Bottoni C, Scanu J, Chiavacci L, Iezzi G. The Pradtlplane aircraft configuration. *Aerodays*, Wien, 2006.

[5] Kroo I. Nonplanar wing concepts for increased aircraft efficiency. *Innovative configurations and advanced concepts for future civil aircraft,* von Karman Institute, Brussels, Belgium, 2005.

[6] Prandtl L. *Induced drag of multiplanes.* NACA TN 182, 1924.

[7] Gall PD. *An experimental and theoretical analysis of the aerodynamics characteristics of a biplane-winglet configuration.* NASA TM 85815, 1984.

[8] Nenadovitch M. *Recherches sur les cellules biplanes rigides d'envergure infine*, Institut Aerotechnique de Saint-Cyr, 1936.

[9] Norton F. *The effect of staggering a biplane,* NACA TN 70, 1921.

[10] Knight M, Noyes R. *Wind tunnel tests on a series of biplane wing models, Part I*, NACA TN 310, 1929.

[11] Knight M, Noyes R. *Wind tunnel tests on a series of biplane wing models, Part II*, NACA TN 325, 1929.

[12] Knight M, Noyes R. *Wind tunnel tests on a series of biplane wing models, Part III*, NACA TN 330, 1929.

[13] Barcala M, Cuerno-Rejado C, del Giudice S, Gandía-Agüera F, Rodríguez-Sevillano, AA. Experimental investigation on box-wing configuration for UAS. *26th Bristol International Unmanned Air Vehicle Systems Conference,* University of Bristol, 11-13 April 2011.

[14] Drela M, Youngren H. Athena Vortex Lattice. Massachusetts Institute of Technology.

[15] Jones B. *Elements of practical aerodynamics.* Wiley, New York, 1950.

Copyright Statement